Journal of King Saud University – Science 31 (2019) 1388–1398

Contents lists available at ScienceDirect

Journal of King Saud University – Science

journal homepage: www.sciencedirect.com

Hydrodynamic stability and heat and mass transfer flow analysis of MHD radiative fourth-grade fluid through porous plate with chemical reaction

S.M. Arifuzzaman [a], Md. Shakhaoath Khan [b,*], Abdullah Al-Mamun [c], Sk. Reza-E-Rabbi [d], Pronab Biswas [d], Ifsana Karim [e]

[a] Centre for Infrastructure Engineering, Western Sydney University, NSW 2751, Australia
[b] School of Engineering, RMIT University, VIC 3001, Australia
[c] Physics Discipline, Khulna University, Khulna 9208, Bangladesh
[d] Mathematics Discipline, Khulna University, Khulna 9208, Bangladesh
[e] Discipline of Chemical Engineering, University of Newcastle, NSW-2308, Australia

ARTICLE INFO

Article history:
Received 21 September 2018
Accepted 31 December 2018
Available online 2 January 2019

Keywords:
Fourth-grade fluid
Heat and mass transport
Chemical reaction
EFDM
Stability analysis

ABSTRACT

Present report intends to analyse heat and mass transfer characteristics of naturally convective hydromagnetic flow of fourth-grade radiative fluid resulting from vertical porous plate. The impression of non-linear order chemical reaction and heat generation with thermal diffusion are also considered. The coupled fundamental equations are transformed into a dimensionless arrangement by implementing finite difference scheme explicitly. After initiating the stability test, the governing equations are converged for Prandtl number, $P_r \geq 0.43$ and Schmidt number, $S_c \geq 0.168$. The impact of dimensionless second, third and fourth-grade parameters with diversified physical parameters are being exhibited graphically on different flow fields. An interesting fact is observed that as the grade of fluid develops it starts to diminish the velocity fields, but a complete opposite scenario is examined for temperature fields. In addition, for advanced visualisation, the impression of thermal radiation is being observed through streamlines and isothermal lines. In which, the respective parameter upsurges the momentum as well as the thermal boundary layers respectively.
© 2018 The Authors. Production and hosting by Elsevier B.V. on behalf of King Saud University. This is an open access article under the CC BY-NC-ND license (http://creativecommons.org/licenses/by-nc-nd/4.0/).

1. Introduction

A vast scientific analysis of non-Newtonian fluid flow problems on heat and mass transfer has done by many researchers. It has an extensive range of impact on different sectors like power engineering, metallurgy, astrophysics and geophysics. The fourth-grade fluid flow model is exceptional model which has opened a new subway of fluid mechanics. This sort of model is being used to explain the flow attitude of non-Newtonian fluids. Second-grade fluid model exhibits variations of normal stress; these sorts of fluids do not consider shear-thickening and thinning phenomena because they exert constant shear viscosity. With the analysis of third and fourth-grade fluids, the results can be described well for shear thinning and shear thickening phenomena. Generally, non-Newtonian fluids are categorised into three types which are namely differential, rate and integral. Fourth-grade fluid is an important subclass of differential type that's capable of describing shear thinning and shear thickening effects. However, despite involving a large number of complex parameter in a Fourth-grade fluid, Hayat et al. (2002) have experimented this by the effect of uniform magnetic field combined with steady and unsteady flows over a porous plate. They used differential equation of order six for a numerical solution with a total three boundary conditions related with momentum and finite difference. Lie point symmetries were applied by Hayat et al. (2002) to reduce the number and order of distinct variable of partial differential equations. Here, they have worked only unsteady of similar fluid past on porous plate. The properties of non-Newtonian fluids have attracted numerous scientists (Asghar et al., 2007; Eldabe et al., 2016; Eldahab and Salem, 2005; Ezzat, 2010) in recent times. Applesauce, tomato ketchup, shampoos contain the properties of

* Corresponding author.
E-mail addresses: 19243001@student.westernsydney.edu.au (S.M. Arifuzzaman), mohammad.shakhaoath.khan@rmit.edu.au (M.S. Khan), mamun101730@gmail.com (A. Al-Mamun), rezarabbi06@gmail.com (Sk. Reza-E-Rabbi), pronabbiswas16@gmail.com (P. Biswas), ifsana.karim@uon.edu.au (I. Karim).
Peer review under responsibility of King Saud University.

Production and hosting by Elsevier

https://doi.org/10.1016/j.jksus.2018.12.009
1018-3647/© 2018 The Authors. Production and hosting by Elsevier B.V. on behalf of King Saud University.
This is an open access article under the CC BY-NC-ND license (http://creativecommons.org/licenses/by-nc-nd/4.0/).

Nomenclature

$B_\circ$	magnetic component, (Wb m^{-2})
C_f	local skin-friction, (–)
C_p	specific heat at constant pressure, (J kg^{-1} K^{-1})
N_u	local Nusselt number, (–)
P_r	Prandtl number, (–)
q_r	unidirectional radiative heat flux, (kg m^{-2})
S_c	Schmidt number, (–)
S_h	local Sherwood number, (–)
T	fluid temperature, (K)
T_w	temperature at the plate surface, (K)
T_∞	ambient temperature as y tends to infinity, (K)
$U_\circ$	uniform velocity u, v velocity components
x, y	cartesian co-ordinates
Greek symbols	
α	dimensionless second-grade fluid parameter
β, β_A	dimensionless third-grade fluid parameter
β_T	thermal expansion co-efficient
β_C	concentration expansion co-efficient
γ, γ_A	dimensionless fourth-grade fluid parameter
κ	thermal conductivity, (W m^{-1} K^{-1})
μ	dynamic viscosities
ρ	density of the fluid, (kg m^{-3})
σ_s	Stefan-Boltzmann constant, 5.6697×10^{-8} (W m^{-2} K^{-4})
ν	kinematic viscosity, (m^2 s^{-1})

non-Newtonian fluid. The non-Newtonian fluid flow model of non-linear coupled differential equations was solved (Sahoo and Poncet, 2013) with shooting and Broyden's method. By assembling the impressions of thermal radiation and thermo-diffusion (Bhatti and Rashidi, 2016) examined the attitude of Williamson nanofluid which was flowing from the stretched surface. Bhatti et al. (2018) observed the bioheat and mass transfer phenomena for dual phase flow of peristaltic propulsion via Darcy-Brinkman-Forchheimer porous media. In recent times, (Ellahi et al., 2018a; Ellahi et al., 2018b) investigated the impression of nano liquid namely kerosene-alumina on hydromagnetic Poiseuille flow. In addition, the impact of entropy generation was also examined with slip influence on moving plate. The pioneer work of representing the combine impressions of magnetic and porous term for diversified motions was exhibited by Fetecau et al. (2018).

Moreover, (Hassan et al., 2017; Reza-E-Rabbi et al., 2018; Hassan et al., 2018a; Hassan et al., 2018b) investigated diversified base fluids with different nanoparticles to develop the area of heat transfer. Considering the impact of electro-magnetohydrodynamics the flow character of multiphase fluids were analysed by Hussain et al. (2018) in a base fluid with the appearance of hafnium particles. However, some reputed researchers (Khan et al., 2018; Majeed et al., 2018; Mishra et al., 2017; Shahid et al., 2017) developed the heat transfer as well as mass transfer phenomena for various fluids flow on different surfaces in the very recent period. For examining the character of blood flow, (Shahid et al., 2018) conducted their experiment via a capillary with the appearance of gyrotactic microorganisms. The model of Couette-Poiseuille flow was established by Shehzad et al. (2018) to analyse aluminium oxide-PVC nanofluid in a channel. Envisaging the impact of hydromagnetic bio-bi-phase flow, (Zeeshan et al., 2018) exhibited the peristaltic transportation of Jeffery fluid in a quadrate duct.

Diversified fluid models have been mentioned to analyse non-Newtonian fluids attitude. A characteristic comparison between non-Newtonian fluid of 4th grade and Newtonian fluid had been analysed by Wang and Wu (2007) and studied numerically of this fluid in case of unsteady MHD flow to an oscillating plate by using finite difference method to solve higher order non-linear partial differential equation after considering four asymptotic boundary conditions. The recent work on comparing with analytical and numerical by Aziz and Mahomed (2013), they have been investigated reduction and solution of unsteady fourth-grade fluid on porous pate by using translational symmetries. Arifuzzaman et al. (2017a) analysed chemically reactive viscoelastic with nanoparticle over porous stretching sheet by imposing explicit scheme. Similar method was applied to micropolar fluid, Jeffrey nanofluid, optically grey-nanofluid by considering different conditions with convergence test (Arifuzzaman et al., 2018a; Arifuzzaman et al., 2017b; Arifuzzaman et al., 2018b; Arifuzzaman et al., 2017c; Biswas et al., 2017; Biswas et al., 2018; Khan et al., 2012a). In recent eras, the study of radiation absorption (Arifuzzaman et al., 2017b; Arifuzzaman et al., 2018b; Biswas et al., 2017; Umamaheswar et al., 2016) and heat generation (Khan et al., 2012b; Khan et al., 2017; Li et al., 2016; Srinivasa and Eswara, 2016) due to mass and heat transfer in fluid flow is industrially significant because of engineering and manufacturing needs for example heat insulation, geothermal systems, combustion, metal waste, catalytic reactors, reactor safety, oil reservoirs, etc.

To author's best knowledge, the investigation of naturally convective fourth grade radiative fluid flow resulting from infinite perpendicular porous plate has not done yet. Therefore, this phenomenon is analysed in this work. The specific objectives of this numerical investigation are listed below:

- To analyse unsteady naturally convective mass and heat transfer flow of fourth grade radiative fluid resulting from infinite perpendicular porous plate by considering non-linear order chemical reaction and heat generation with thermal diffusion.
- To establish a mathematical solution of the flow governing model which includes transient momentum, diffusion balance and energy equations and solve it by employing finite difference scheme explicitly.
- To present a details stability and convergence study for optimising appropriate parameters.
- To exhibit velocity, temperature and concentric fields graphically along with Nusselt number, skin friction and Sherwood number profiles.
- To represent the tabular analysis of C_f, N_u, and S_h fields for a steady-state solution.
- To present the advanced visualisation of fluid flow through streamlines and Isothermal lines.

2. The mathematical fluid flow model

A naturally convective and thermally radiative incompressible simple fourth-grade fluid is defined for unsteady case model, and the fluid is passing through a vertical infinite porous plate with destructive chemical reaction and heat generation effect (Fig. 1). With the history of the deformation gradient, the current stress of an element is constituted for an incompressible fluid flow model, and it can be exhibited as,

$$M(x,t) = pI + S^{\infty}_{K=0}(S^{t}_{t}(K)) \quad (1)$$

Where, pI = indeterminate portion of stress–tensor and S = deformation gradient. Coleman and Noll (1960), prescribed different sort of incompressible fluid of category n as viscous fluid agreeing on the following equation (Hayat et al., 2002; Sahoo and Poncet, 2013),

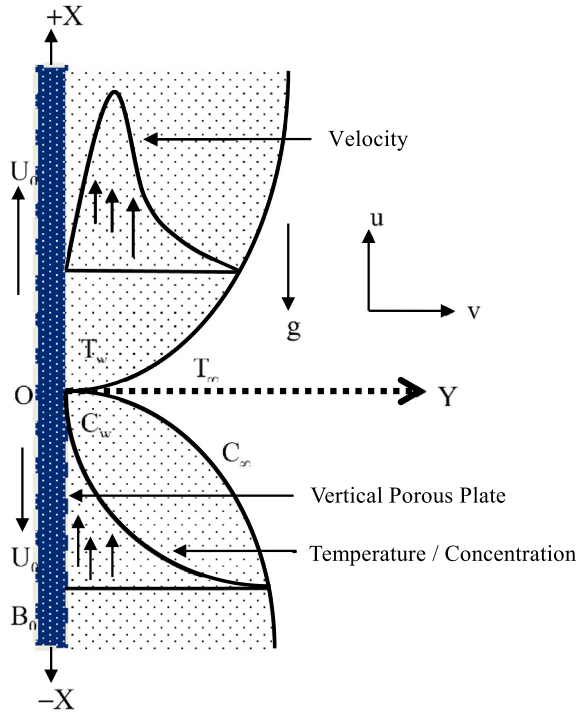

Fig. 1. The physical configuration of the flow.

$$M(x,t) = -pI + \sum_{j=1}^{n} K_j \tag{2}$$

The asymptotic expansion is being employed for functional in Eq. (1) via an obstacle parameter and the tensors K_j are achieved for n = 4 as (Hayat et al., 2011, 2002; Sahoo and Poncet, 2013),

$$K_1 = \mu L_1 \tag{3}$$

$$K_2 = \alpha_1 L_2 + \alpha_2 L_1^2 \tag{4}$$

$$K_3 = \beta_1 L_3 + \beta_2 (L_1 L_2 + L_2 L_1) + \beta_3 (\mathrm{tr} L_3^2) L_1 \tag{5}$$

$$K_4 = \gamma_1 L_4 + \gamma_2 (L_3 L_2 + L_1 L_3) + \gamma_3 L_2^2 + \gamma_4 (L_2 L_1^2 + L_1^2 L_2) + \gamma_5 (\mathrm{tr} L_2) L_2 + \gamma_6 (\mathrm{tr} L_2) L_1^2 + [\gamma_7 \mathrm{tr} L_3 + \gamma_8 \mathrm{tr}(L_2 L_1)] L_1 \tag{6}$$

Here, μ = shear-viscosity coefficient, $\alpha_i (i = 1, 2) = \beta_i (i = 1, 2, 3) = \gamma_i (i = 1, 2, \ldots 8)$ = material constants and I = identity tensor. Here, for 4th-grade fluid, Cauchy stress tensor ***M*** can be exhibited as,

$$M = -pI + \mu L_1 \alpha_1 L_2 + \alpha_2 L_1^2 + \beta_1 L_3 + \beta_2 (L_1 L_2 + L_2 L_1) + \beta_3 (\mathrm{tr} L_3^2) L_1 + \gamma_1 L_4 + \gamma_2 (L_3 L_2 + L_1 L_3) + \gamma_3 L_2^2 + \gamma_4 (L_2 L_1^2 + L_1^2 L_2) + \gamma_5 (\mathrm{tr} L_2) L_2 + \gamma_6 (\mathrm{tr} L_2) L_1^2 + [\gamma_7 \mathrm{tr} L_3 + \gamma_8 \mathrm{tr}(L_2 L_1)] L_1 \tag{7}$$

The Rivlin–Ericksen tensors (L_n) are prescribed by following recursion connection:

$$L_n = \frac{dL_{n-1}}{dt} + L_{n-1}(\mathrm{grad}\, V) + (\mathrm{grad} V)^T L_{n-1}, \; n > 1;$$
$$L_1 = (\mathrm{grad}\, V) + (\mathrm{grad} V)^T \tag{8}$$

A third-grade model is achieved when n = 3 in Eq. (2) and $\gamma_i = 0$. For n = 2 in Eq. (2), $\beta_i = 0$ and $\gamma_i = 0$ a second-grade fluid is adopted, and the above-discussed model becomes a usual Navier-Stokes fluid for $\alpha_i = 0$, $\beta_i = 0$ and $\gamma_i = 0$ (i.e. n = 1 in (2)). The thermally radiative and chemically reactive flow is heading in x-direction along infinite porous plate with heat generation. Here, U_0 is the uniform velocity where T_∞ and C_∞ are fluid temperature and concentration away from the layer. A uniform magnetic field $(B_x = 0, B_y = B_0)$ is imposed in the normal direction of the flow. Under the above consideration, the equations that described the physical circumstances are given below (Arifuzzaman et al., 2018b,c; Gul et al., 2016; Hayat et al., 2011; Wang and Wu, 2007):

Continuity Equation,

$$\frac{\partial v}{\partial y} = 0 \tag{9}$$

Momentum Equation,

$$\frac{\partial u}{\partial t} + v\frac{\partial u}{\partial y} = \upsilon \frac{\partial^2 u}{\partial y^2} + \frac{\alpha_1 \upsilon}{\rho}\frac{\partial^3 u}{\partial y^2 \partial t} + \frac{\beta_1 \upsilon^2}{\rho}\frac{\partial^4 u}{\partial y^2 \partial t^2} + \frac{6(\beta_2+\beta_3)}{\rho}\left(\frac{\partial u}{\partial y}\right)^2 \frac{\partial^2 u}{\partial y^2} + \frac{\gamma_1 \upsilon^3}{\rho}\frac{\partial^5 u}{\partial y^2 \partial t^3} + \frac{2\upsilon(3\gamma_2+\gamma_3+\gamma_4+\gamma_5+3\gamma_7+\gamma_8)}{\rho}\left[2\frac{\partial u}{\partial y}\frac{\partial^2 u}{\partial y^2}\frac{\partial^2 u}{\partial y \partial t} + \left(\frac{\partial u}{\partial y}\right)^2 \frac{\partial^3 u}{\partial y^2 \partial t}\right] - \frac{\sigma B_0^2}{\rho}u + g\beta_T(T_w - T_\infty) + g\beta_C(C_w - C_\infty) - \frac{\upsilon}{k}u \tag{10}$$

Energy Equation,

$$\frac{\partial T}{\partial t} + v\frac{\partial T}{\partial y} = \frac{\kappa}{\rho c_p}\frac{\partial^2 T}{\partial y^2} + \frac{\upsilon}{c_p}\left(\frac{\partial u}{\partial y}\right)^2 + \frac{\alpha_1 \upsilon}{\rho c_p}\frac{\partial^2 u}{\partial y \partial t}\frac{\partial u}{\partial y} + \frac{\beta_1 \upsilon^2}{\rho c_p}\frac{\partial^3 u}{\partial y \partial t^2} \times \frac{\partial u}{\partial y} + \frac{2(\beta_1+\beta_3)}{c_p \rho}\left(\frac{\partial u}{\partial y}\right)^4 + \frac{\gamma_1 \upsilon^3}{\rho c_p}\frac{\partial^4 u}{\partial y^2 \partial t^2}\frac{\partial u}{\partial y} + \frac{2\upsilon(3\gamma_2+\gamma_3+\gamma_4+\gamma_5+3\gamma_7+\gamma_8)}{\rho c_p}\frac{\partial^2 u}{\partial y \partial t}\left(\frac{\partial u}{\partial y}\right)^3 + \frac{Q_0}{\rho c_p}(T_w - T_\infty) - \frac{1}{\rho c_p}\frac{\partial q_r}{\partial y} \tag{11}$$

Concentration Equation,

$$\frac{\partial C}{\partial t} + v\frac{\partial C}{\partial y} = D_m\left(\frac{\partial^2 C}{\partial y^2}\right) + \frac{D_m \kappa_T}{c_s c_p}\frac{\partial^2 T}{\partial y^2} - K_c(C - C_\infty)^p \tag{12}$$

with boundary condition,

$$u = 0, \; T = T_w, \; C = C_w \text{ at } \; y = 0$$
$$u = 0, T \to T_\infty, \; C \to C_\infty \text{ at } \; y \to \infty \tag{13}$$

Here, $q_r = -(4\sigma_s/3k_e)\left(\partial T^4/\partial y\right)$ is the Rosseland approximation for radiative heat flux. The temperature differences are chosen small inside the flow. Then expanding T^4 by approximating Taylor series at T_∞, it is adopted that $T^4 \cong 4T_\infty^3 T - 3T_\infty^4$ (higher terms are deducted).

Then the Eq. (11) becomes,

$$\frac{\partial T}{\partial t} + v\frac{\partial T}{\partial y} = \frac{\kappa}{\rho c_p}\frac{\partial^2 T}{\partial y^2} + \frac{\upsilon}{c_p}\left(\frac{\partial u}{\partial y}\right)^2 + \frac{\alpha_1 \upsilon}{\rho c_p}\frac{\partial^2 u}{\partial y \partial t}\frac{\partial u}{\partial y} + \frac{\beta_1 \upsilon^2}{\rho c_p}\frac{\partial^3 u}{\partial y \partial t^2} \times \frac{\partial u}{\partial y} + \frac{2(\beta_2+\beta_3)}{c_p \rho}\left(\frac{\partial u}{\partial y}\right)^4 + \frac{\gamma_1 \upsilon^3}{\rho c_p}\frac{\partial^4 u}{\partial y^2 \partial t^2}\frac{\partial u}{\partial y} + \frac{2\upsilon(3\gamma_2+\gamma_3+\gamma_4+\gamma_5+3\gamma_7+\gamma_8)}{\rho c_p}\frac{\partial^2 u}{\partial y \partial t}\left(\frac{\partial u}{\partial y}\right)^3 + \frac{Q_0}{\rho c_p}(T_w - T_\infty) + \frac{16\sigma_s T_\infty^3}{3k_e \rho c_p}\frac{\partial^2 T}{\partial y^2} \tag{14}$$

To find the solutions of the governing Eqs. (9)–(14) the non-dimensional quantities are adopted as:

$$Y = \frac{yU_0}{\upsilon}, \; U = \frac{u}{U_0}, \; \tau = \frac{tU_0^2}{\upsilon}, \; \theta = \frac{T - T_\infty}{T_w - T_\infty}, \; \phi = \frac{C - C_\infty}{C_w - C_\infty}, \; V = \frac{v}{U_0} \tag{15}$$

Continuity Equation,

$$\frac{\partial v}{\partial y} = 0 \Rightarrow v = -v_0 \tag{16}$$

where, $v_0 > 0$ and $v_0 < 0$ are suction and injection velocity. Here, $v_0 > 0$ is considered.

Momentum Equation,

$$\begin{aligned}\frac{\partial U}{\partial \tau} - S\frac{\partial U}{\partial Y} = {} & \frac{\partial^2 U}{\partial Y^2} + G_r\theta + G_c\phi - MU - \frac{1}{D_a}U + \alpha\frac{\partial^3 U}{\partial Y^2\partial\tau} \\ & + \beta\frac{\partial^4 U}{\partial Y^2\partial\tau^2} + \beta_A\left(\frac{\partial U}{\partial Y}\right)^2\frac{\partial^2 U}{\partial Y^2} + \gamma_A\frac{\partial^5 U}{\partial Y^2\partial\tau^3} \\ & + \gamma\left[2\frac{\partial U}{\partial Y}\frac{\partial^2 U}{\partial Y^2}\frac{\partial^2 U}{\partial Y\partial\tau} + \left(\frac{\partial U}{\partial Y}\right)^2\frac{\partial^3 U}{\partial Y^2\partial\tau}\right]\end{aligned} \tag{17}$$

Energy Equation,

$$\begin{aligned}\frac{\partial\theta}{\partial\tau} - S\frac{\partial\theta}{\partial Y} = {} & \frac{1}{P_r}\left(1 + \frac{16R}{3}\right)\frac{\partial^2\theta}{\partial Y^2} + Q\theta + E_c\left(\frac{\partial U}{\partial Y}\right)^2 \\ & + E_c\left[\alpha\frac{\partial^2 U}{\partial Y\partial\tau}\frac{\partial U}{\partial Y} + \beta\frac{\partial^3 U}{\partial Y\partial\tau^2}\frac{\partial U}{\partial Y} + \beta_A\left(\frac{\partial U}{\partial Y}\right)^4\right. \\ & \left. + \gamma_A\frac{\partial^4 U}{\partial Y^2\partial\tau^2}\frac{\partial U}{\partial Y} + \gamma\frac{\partial^2 U}{\partial Y\partial\tau}\left(\frac{\partial U}{\partial Y}\right)^3\right]\end{aligned} \tag{18}$$

Concentration Equation,

$$\frac{\partial\phi}{\partial\tau} - S\frac{\partial\phi}{\partial Y} = \frac{1}{S_c}\frac{\partial^2\phi}{\partial Y^2} + S_r\frac{\partial^2\theta}{\partial Y^2} - K_r\phi^p \tag{19}$$

with boundary condition,

$$\begin{aligned} & U = 0,\ T = 1,\ C = 1 \quad \text{at } y = 0 \\ & U = 0,\ T = 0,\ C = 0 \quad \text{at } y \to \infty\end{aligned} \tag{20}$$

where the dimensionless parameters are: Suction parameter, $S = v_0/U_0$, Grashof number, $G_r = g\beta_T(T_w - T_\infty)\upsilon/U_0^3$, mass Grashof number, $G_c = g\beta_C(C_w - C_\infty)\upsilon/U_0^3$, magnetic parameter, $M = \sigma' B_0^2\upsilon/\rho U_0^2$, second-grade fluid parameter, $\alpha = \alpha_1 U_0^2/\rho\upsilon^2$, third-grade fluid parameters, $\beta = \beta_1 U_0^4/\rho\upsilon^3$, $\beta_A = 6(\beta_2 + \beta_3)U_0^4/\rho\upsilon^3$, fourth-grade fluid parameter, $\gamma_A = \gamma_1 U_0^6/\rho\upsilon^4$, $\gamma = 2(3\gamma_2 + \gamma_3 + \gamma_4 + \gamma_5 + 3\gamma_7 + \gamma_8)U_0^6/\rho\upsilon^4$, Darcy number, $D_a = kU_0^2/\upsilon^2$, radiation parameter, $R = \sigma T_\infty^3/k_1 k$, heat source parameter, $Q = Q_0\upsilon/U_0^2\rho\, c_p$, Prandtl number, $P_r = \rho\, c_p\upsilon/\kappa$, Eckert number, $E_c = U_0^2/c_p(T_w - T_\infty)$, Schmidt number, $S_c = D_m/\upsilon$, order of chemical reaction = P, Soret number, $S_r = D_m\kappa_T(T_w - T_\infty)/T_m\upsilon(C_w - C_\infty)$ and chemical reaction, $K_r = \upsilon K_c(C_w - C_\infty)^{p-1}/U_0^2$.

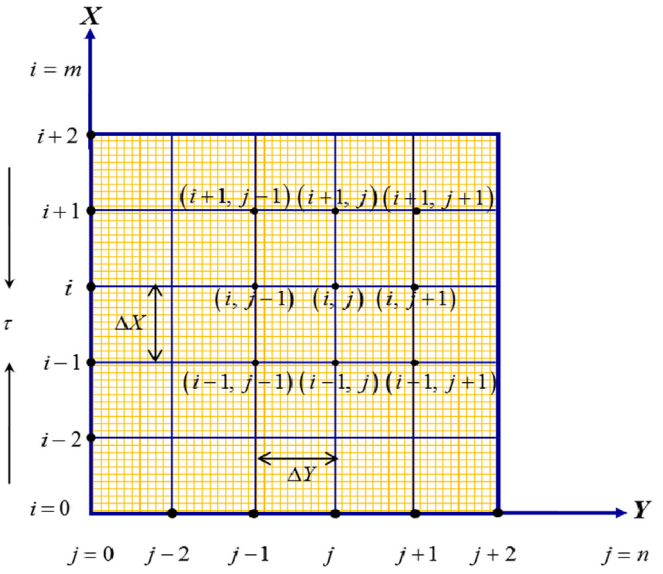

Fig. 2. Numerical grid setup.

In addition, the physical momentum, heat and mass properties such as skin-friction, the Nusselt and Sherwood number, which are elucidated as (Arifuzzaman et al., 2018b),

$$\left.\begin{aligned} C_f &= -\tfrac{1}{2\sqrt{2}}G_r^{-3/4}\left(\tfrac{\partial U}{\partial Y}\right)_{Y=0}, \\ N_u &= \tfrac{1}{\sqrt{2}}G_r^{-3/4}\left(\tfrac{\partial\theta}{\partial Y}\right)_{Y=0}, \\ S_h &= \tfrac{1}{2\sqrt{2}}G_r^{-3/4}\left(\tfrac{\partial\phi}{\partial Y}\right)_{Y=0}. \end{aligned}\right\} \tag{21}$$

3. Numerical solution

Explicit finite difference technique is being performed for resolving Eqs. (16)–(20) within conferred boundary conditions. A rectangular flow field is adapted for distributing the grid lines which are collateral to X and Y axes (Fig. 2). For the current inquiry, the following things are chosen as,

Grid space: m = 200, n = 200, Plates height: $X_{max} = 15$, $Y_{max} = 60$ as $Y \to \infty$,

Mesh sizes: $\Delta Y = 0.30(0 \leqslant Y \leqslant 50)$ and $\Delta X = 0.075(0 \leqslant X \leqslant 15)$, $\Delta\tau = 0.005$

Now, Eqs. (16)–(20) are changed into the following finite difference form,

$$\frac{U_{i,j} - U_{i-1,j}}{\Delta X} + \frac{V_{i,j} - V_{i,j-1}}{\Delta Y} = 0 \tag{22}$$

Momentum Equation,

$$\begin{aligned}\frac{U'_{i,j} - U_{i,j}}{\Delta\tau} - S\frac{U_{i,j+1} - U_{i,j}}{\Delta Y} = {} & G_r\theta_{i,j} + G_c\phi_{i,j} - \left(M + \frac{1}{D_a}\right)U_{i,j} + \frac{U_{i,j+1} - 2U_{i,j} + U_{i,j-1}}{(\Delta Y)^2} + \alpha\frac{U'_{i,j+1} - 2U'_{i,j} + U'_{i,j-1} - U_{i,j+1} + 2U_{i,j} - U_{i,j-1}}{\Delta\tau(\Delta Y)^2} \\ & + \beta\left[\frac{U''_{I,J+1} - 3U'_{I,J+1} + 2U_{I,J+1} + 2U''_{I,J} - 4U'_{I,J} + 2U_{I,J} + U''_{I,J-1} - U'_{I,J-1}}{\Delta Y^2\Delta\tau^2}\right] + \beta_A\left(\frac{U_{i,j+1} - U_{i,j}}{\Delta Y}\right)^2\frac{U_{i,j+1} - 2U_{i,j} + U_{i,j-1}}{(\Delta Y)^2} \\ & + \gamma_A\frac{\left[U'''_{I,J+1} - 3U''_{I,J+1} + 3U'_{I,J+1} + U_{I,J+1} - 2U'''_{I,J} - 6U''_{I,J} + 6U'_{I,J} + 2U_{I,J} + U'_{I,J-I} - 3U''_{I,J-1} + 3U'_{I,J-1} + U_{I,J-1}\right]}{\Delta Y^2\Delta\tau^3} \\ & + \gamma\left[2\frac{U_{i,j+1} - U_{i,j}}{\Delta Y}\frac{U_{i,j+1} - 2U_{i,j} + U_{i,j-1}}{(\Delta Y)^2}\frac{U'_{i,j+1} - 2U'_{i,j} + U'_{i,j-1} - U_{i,j+1} + 2U_{i,j} - U_{i,j-1}}{\Delta\tau(\Delta Y)^2}\right]\end{aligned} \tag{23}$$

Energy Equation,

$$\frac{\theta'_{i,j}-\theta_{i,j}}{\Delta\tau}-S\frac{\theta_{i,j+1}-\theta_{i-1,j}}{\Delta Y}=\frac{1}{P_r}\left(1+\frac{16}{3}R\right)\frac{\theta_{i,j+1}-2\theta_{i,j}+\theta_{i,j-1}}{(\Delta Y)^2}+Q\theta_{i,j}+E_c\left(\frac{U_{i,j+1}-U_{i,j}}{\Delta Y}\right)^2$$
$$+E_c\left[\alpha\frac{U'_{I,J+1}-U'_{I,J}-U_{I,J+1}+U_{I,J}}{\Delta Y\Delta\tau}\frac{U_{i,j+1}-U_{i,j}}{\Delta Y}+\beta\frac{U''_{I,J+1}-2U'_{I,J+1}+U_{I,J+1}-U''_{I,J}-2U''_{I,J}+2U'_{I,J}-U_{I,J}}{\Delta Y\Delta\tau^2}\frac{U_{I,J+1}-U_{I,J}}{\Delta Y}+\beta_A\left(\frac{U_{i,j+1}-U_{i,j}}{\Delta Y}\right)^4\right.$$
$$\left.+\gamma_A\frac{U''_{I,J+1}-3U'_{I,J+1}+2U_{I,J+1}+2U''_{I,J}-4U'_{I,J}+2U_{I,J}+U''_{I,J-1}-U'_{I,J-1}}{\Delta Y^2\Delta\tau^2}\frac{U_{i,j+1}-U_{i,j}}{\Delta Y}+\gamma\frac{U'_{I,J+1}-U'_{I,J}-U_{I,J+1}+U_{I,J}}{\Delta Y\Delta\tau}\left(\frac{U_{i,j+1}-U_{i,j}}{\Delta Y}\right)^3\right] \quad (24)$$

Concentration Equation,

$$\phi'_{i,j}=\phi_{i,j}+\Delta\tau\left[\frac{1}{S_c}\frac{\phi_{i,j+1}-2\phi_{i,j}+\phi_{i,j-1}}{(\Delta Y)^2}+S_r\frac{\theta_{i,j+1}-2\theta_{i,j}+\theta_{i,j-1}}{(\Delta Y)^2}\right.$$
$$\left.-K_r(\phi_{i,j})^p+S\frac{\phi_{i,j+1}-\phi_{i,j}}{\Delta Y}\right] \quad (25)$$

The initial and boundary condition with a finite difference scheme as,

$$U^n_{i,0}=0,\quad \theta^n_{i,0}=1,\ \phi^n_{i,0}=1$$
$$U^n_{i,L}=0,=\ \theta^n_{i,L}=0,\ \phi^n_{i,L}=0\ \text{where}\ L\to\infty \quad (26)$$

where, the subscripts i and j designate the grid points with X and Y coordinates respectively and value of time,$\tau=n\Delta\tau$, where, $n=1,2,3,4$.....

4. Stability and convergence analysis

The ongoing analysis requires the study of the stability and convergence test because an explicit procedure is being performed. Here, Eqs. (16) is disregarded because $\Delta\tau$ is not available there. The Fourier expansions are attained as in Eqs. (27) and (28) for all U, θ and φ.

$$\left.\begin{array}{l}U:\psi(\tau)e^{i\alpha X}e^{i\beta Y}\\ \theta:\theta(\tau)e^{i\alpha X}e^{i\beta Y}\\ \varphi:\varphi(\tau)e^{i\alpha X}e^{i\beta Y}\end{array}\right\}(\text{at time}\ \tau) \quad (27)$$

and

$$\left.\begin{array}{l}U':\psi'(\tau)e^{i\alpha X}e^{i\beta Y}\\ U'':\psi''(\tau)e^{i\alpha X}e^{i\beta Y}\\ U''':\psi'''(\tau)e^{i\alpha X}e^{i\beta Y}\\ \theta':\theta'(\tau)e^{i\alpha X}e^{i\beta Y}\\ \varphi':\varphi'(\tau)e^{i\alpha X}e^{i\beta Y}\end{array}\right\}(\text{after a time step}) \quad (28)$$

Now, imposing Eqs. (27)–(28) into Eqs. (17)–(20) and choosing U, V as constant we obtain the following equations as;

The momentum equation becomes,

$$\psi'=A_1\psi+A_2\theta+A_3\varphi \quad (29)$$

where,

$$A_1=\left[1-S\frac{\Delta\tau}{\Delta Y}(e^{i\beta\Delta Y}-1)-\left(M+\frac{1}{D_a}\right)\Delta\tau+\frac{\Delta\tau}{(\Delta Y)^2}(\cos\beta\Delta Y-1)\right.$$
$$-\alpha\frac{2(\cos\beta\Delta Y-1)}{(\Delta Y)^2}+\beta\frac{2(e^{i\beta\Delta X}+1)}{\Delta\tau(\Delta Y)^2}$$
$$+\beta_A\frac{2\Delta\tau(\cos\beta\Delta Y-1)}{\Delta Y^2}+\gamma_A\frac{2(\cos\beta\Delta Y-1)}{\Delta\tau^2(\Delta Y)^2}$$
$$\left.-\gamma\frac{2\Delta\tau(e^{i\beta\Delta Y}-1)}{\Delta Y}\frac{2\Delta\tau(\cos\beta\Delta Y-1)}{\Delta Y^2}\frac{2(\cos\beta\Delta Y-1)}{\Delta Y^2}\right.$$
$$\left.-\frac{2(\cos\beta\Delta Y-1)}{\Delta Y^2}\right],\ A_2=G_r\Delta\tau,\ A_3=G_m\Delta\tau. \quad (30)$$

The energy equation becomes,

$$\theta'=A_4\theta(\tau) \quad (31)$$

where,

$$A_4=\left[1-S\frac{\Delta\tau(e^{i\beta\Delta Y}-1)}{\Delta Y}+\frac{\Delta\tau}{P_r}\left(1+\frac{16}{3}R\right)\frac{2(\cos\beta\Delta Y-1)}{(\Delta Y)^2}\right.$$
$$\left.+Q\Delta\tau-\frac{\alpha E_c\psi(\tau)\Delta\tau(e^{i\beta\Delta Y}-1)^2}{\Delta\tau\Delta Y}+\beta\frac{\Delta\tau\psi(\tau)}{\Delta Y^2\Delta\tau}(e^{i\beta\Delta Y}-1)^2\right] \quad (32)$$

And the concentration equation becomes,

$$\varphi'=A_5\phi+A_6\theta \quad (33)$$

where,

$$A_5=1+\left[\frac{1}{Sc}\frac{2\Delta\tau(\cos\beta\Delta Y-1)}{(\Delta Y)^2}+S\frac{\Delta\tau(e^{i\beta\Delta Y}-1)}{\Delta Y}-K_r\Delta\tau\right],$$
$$A_6=Sr\frac{2(\cos\beta\Delta Y-1)}{(\Delta Y)^2}. \quad (34)$$

Eqs. (29), (31) and (33) can be presented in the matrix form as, $\eta'=T\eta$,

$$\begin{bmatrix}\psi'\\ \theta'\\ \varphi'\end{bmatrix}=\begin{bmatrix}A_1 & A_2 & A_3\\ 0 & A_4 & 0\\ 0 & A_6 & A_5\end{bmatrix}\begin{bmatrix}\psi\\ \theta\\ \varphi\end{bmatrix}$$

where,

$$\eta'=\begin{bmatrix}\psi'\\ \theta'\\ \varphi'\end{bmatrix},T=\begin{bmatrix}A_1 & A_2 & A_3\\ 0 & A_4 & 0\\ 0 & A_6 & A_5\end{bmatrix}$$

and

$$\eta=\begin{bmatrix}\psi\\ \theta\\ \varphi\end{bmatrix} \quad (35)$$

Diversified data of T makes the analysis quite hard thus considering $\Delta\tau\to0$, hence, $A_2\to0, A_3\to0$ and $A_6\to0$.∴$T=\begin{bmatrix}A_1 & 0 & 0\\ 0 & A_4 & 0\\ 0 & 0 & A_5\end{bmatrix}$. As a result, the achieved Eigenvalues are $A_1=\lambda_1, A_4=\lambda_2$ and $A_5=\lambda_3$ which satisfy the following stability condition as,

and

$$|A_1|\leqslant1,|A_4|\leqslant1\ \text{and}\ |A_5|\leqslant1 \quad (36)$$

Let,

$$a_1=\Delta\tau,\ d_1=2\frac{\Delta\tau}{(\Delta Y)^2},\ d_2=\frac{\Delta\tau}{\Delta Y},\ d_3=|-S|\frac{\Delta\tau}{\Delta Y}\ \text{and}\ d_4=\frac{\Delta\tau}{\Delta Y^2}$$

where, a_1, d_1, d_2, d_3 and d_4 are real non-negative numbers and $\alpha\Delta X=m\pi$, $\beta\Delta Y=n\pi$.

Now, using Eq. (36) and considering the assumed criterions, A_4 and A_5 are attained as,

$$A_4 = 1 - 2\left[\frac{d_3}{2} + d_1\frac{1}{P_r}\left(1 + \frac{16}{3}R\right) + \frac{Q}{2}a_1 - \frac{\alpha E_c}{2}d_2 + \frac{\beta}{2}d_4\right],$$

$$A_5 = 1 - 2\left[d_1\frac{1}{Sc} + \frac{d_3}{2} - \frac{a_1}{2}K_r\right].$$

The allowable maximum negative numbers are $A_1 = -1$, $A_4 = -1$ and $A_5 = -1$. Thus, the stability criterion is established as,

$$\frac{2\Delta\tau}{P_r(\Delta Y)^2}\left(1 + \frac{16}{3}R\right) + \frac{Q\Delta\tau}{2} + \frac{S\Delta\tau}{\Delta Y} - \frac{\alpha E_c}{2}\frac{\Delta\tau}{\Delta Y} + \frac{\beta\Delta\tau}{2\Delta Y^2} \leqslant 1, \frac{2\Delta\tau}{Sc(\Delta Y)^2} + \frac{S\Delta\tau}{\Delta Y} - \Delta\tau K_r \leqslant 1.$$

For, $U = V = T = C = 0$ together with the data of $\Delta\tau = 0.005$ and $\Delta Y = 0.30$ the existing work is converged for $P_r \geqslant 0.43$ and $Sc \geqslant 0.168$.

5. Results and discussion

Theoretical work on the laminar flow of fourth-grade fluid has been investigated numerically. The study has been analysed on thermally radiative, and chemically reactive convective fourth-grade fluid flow over a vertical infinite porous plate with the effect of heat source, magnetic field and viscous dissipation has been studied numerically. To validate the present numerical analysis, a numerical comparison is provided in Table 1. It can be seen that the present simulation can predict the previous results with an insignificant deviation. Moreover, the impression of system parameters on C_f, N_u, and S_h are also investigated in Table 2.

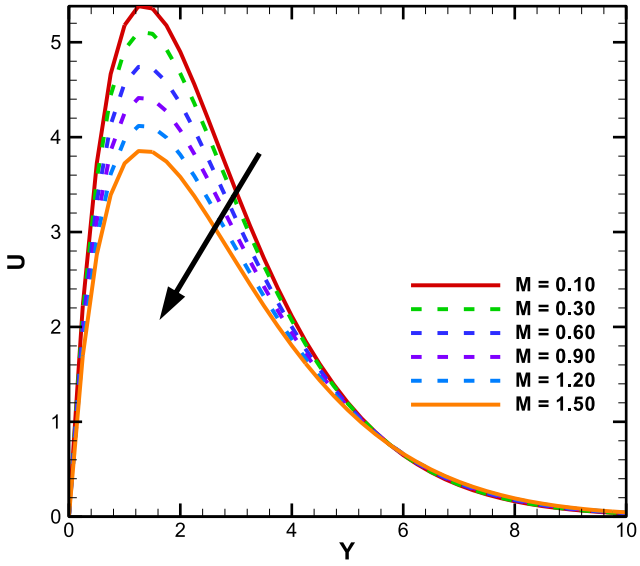

Fig. 3. Dominance of M on U.

The impact of diversified physical parameters along with dimensionless second-grade, third-grade and fourth-grade parameters are depicted graphically on different flow fields. The default values for the pertinent parameters are taken as Ec = 0.0001, Sc = 0.50, Pr = 0.71, α = 0.20, β = 0.05, β_A = 0.05, γ = 0.05, γ_A = 0.05, R = 0.05, Sr = 0.003, Kr = 0.50, Da = 1.0, Gr = 10.0, Gc = 5.0, S = 0.10, M = 0.30. In addition, for advanced visualization of fluid, streamlines and isotherms are also exhibited. The interaction of electrically

Table 1
Validation of present study against Sahoo and Poncet (2013), where $G_r = G_c = 1.0$, $D_a = 10$, $R = 0.05$, $Q = K_r = 0.06$, $S_c = 0.6$, $S_r = 0.003$.

α	β	γ	P_r	M	E_c	Non-dimensional temperature (Sahoo and Poncet, 2013)	Non-dimensional temperature (Present work)
0.01						0.043378	0.04304
0.02	1.0	2.0	2.0	1.0	1.0	0.043233	0.04351
0.03						0.043090	0.04308
		1.0				0.026147	0.02530
2.0	1.0	1.5	1.0	1.0	0.3	0.026142	0.02249
		2.0				0.026137	0.02107
			1.0			0.020760	0.02089
3.0	1.0	2.0	2.0	1.0	0.5	0.020759	0.02074
			3.0			0.020757	0.02023

Table 2
Computational values of C_f, N_u, and S_h for variation of flow parameters for a steady-state solution.

S	R	M	P_r	α	β	γ	Kr	S_c	C_f	N_u	S_h
0.20	0.05	0.30	0.71	0.05	0.05	0.05	0. 50	0.50	0.16788	0.49308	0.61085
0.30									0.18042	0.46521	0.59553
0.40	0.10								0.19254	0.58207	0.44022
0.50	0.15								0.20423	0.41780	0.57015
	0.20	0.60							0.24553	0.39764	0.55949
		0.80							0.22167	0.37984	0.53648
		1.00	1.00						0.21822	0.31149	0.51186
			1.50						0.32467	0.29147	0.67940
			2.00	0.10	0.10				0.30946	0.29013	0.62314
0.80				0.20	0.20				0.45349	0.47985	0.82461
				0.30	0.30	0.10			0.43687	0.56348	0.83454
						0.20			0.41886	0.65942	0.85431
						0.30	1.0		0.39424	0.64875	0.84754
							1.50	0.70	0.64263	0.53185	0.77892
							2.0	0.80	0.71631	0.49821	0.74651
								1.20	0.89300	0.41235	0.67135

conducting fluids with magnetic fields, through electromagnetic forces called Lorentz forces. Strong magnetic parameter (M) creates retarding force namely Lorentz force which diminishes fluid velocity.

Fig. 3 depicts the drag force effect on fluid flow and decreases the velocity profiles with the increase ($0.10 \leqslant M \geqslant 1.50$) of the magnetic parameter (M). The Curve to curve fluctuation for velocity profiles declines 23.025%, 22.53%, 22.17%, 21.80% and 21.46% as M changes from 0.10 to 1.50 respectively at $\tau = 4.0$. Physically, as the intensity of the magnetic field develops a resistive force namely, Lorentz force occurs and impedes the fluid motion. Skin friction behaviour occurred because of the friction loss is the reduction of pressure that happens inside the pipe for the impression of fluid's viscosity close to the surface of the pipe.

Fig. 4 illustrates the skin friction profiles for the increment of magnetic parameter (M). The fields of C_f plunge with rising data of M because the imposed magnetic field tends to decelerate the fluid flows and hence the surface friction force declines.

For the increase of higher order material parameters, elastic characteristics deformation leads to the changes of shape or size of fluid due to an applied force or transformation of heat. For the increase of viscoelastic property, the momentum boundary layer thickness becomes more conservator with the plate, for this reason, velocity profiles decrease. With the rise of higher order material parameters, the viscoelasticity property enhances the molecular particles gathering and temperature absorption rate increase. As a result, the fluid region temperature increases for higher order material parameters.

Figs. 5 and 6 demonstrate the velocity and temperature fields due to the increment ($0.50 \geqslant \alpha \geqslant 3.50$) of the dimensionless second-grade fluid parameter (α). Velocity profiles diminish, and temperature fields increase for the upsurging second-grade fluid

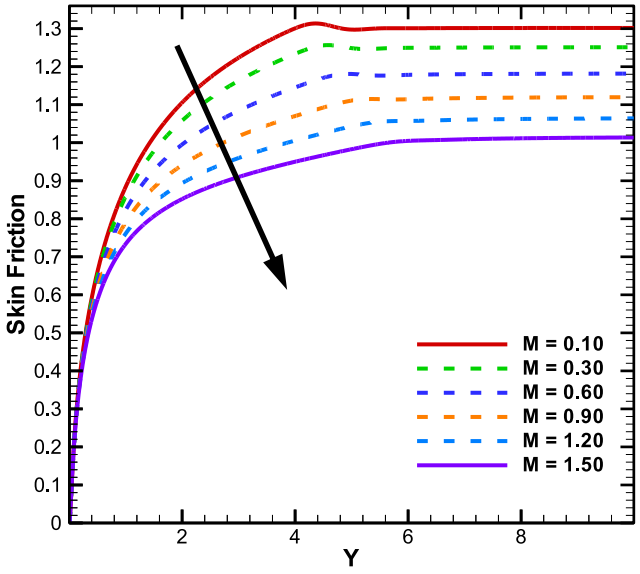

Fig. 4. Dominance of M on C_f.

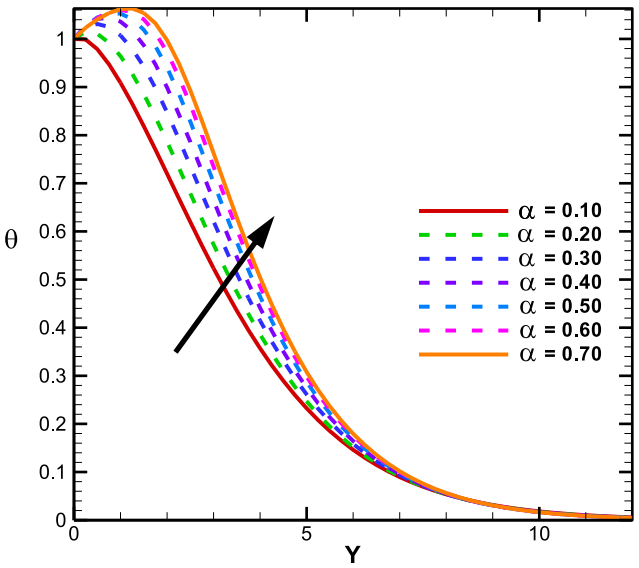

Fig. 6. Dominance of α on θ.

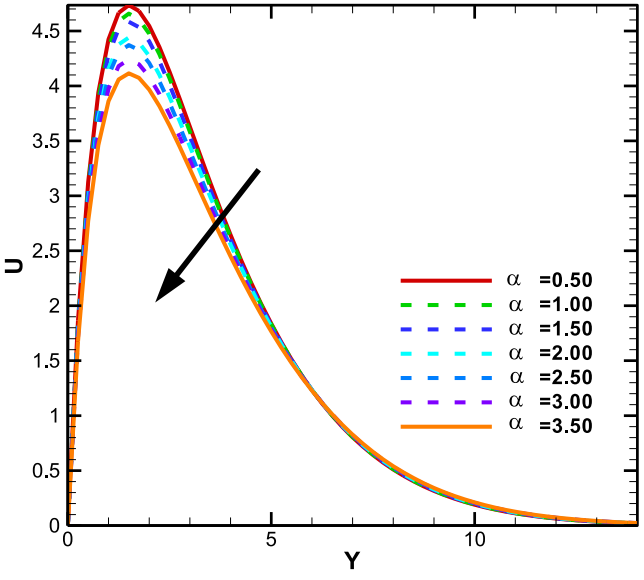

Fig. 5. Dominance of α on U.

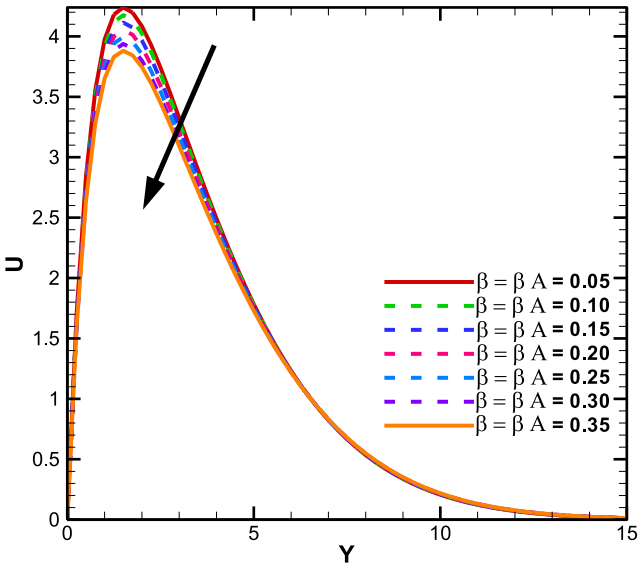

Fig. 7. Dominance of β and β_A on U.

parameter (α). Curve to curve fluctuation of velocity profile with the variation forα at $\tau = 3.0$and 9.24%, 8.97%, 17.48%, 8.51%, 16.59 and 16.03% changes for increment of 0.5 (0.50–3.50).

Figs. 7 and 8 depict the impact of third-grade fluid parameters ($0.05 \leqslant (\beta = \beta_A) \geqslant 0.35$) on velocity and temperature fields. Velocity fields diminish, and temperature fields develop with the increase of third-grade fluid parameter (β and β_A).

Figs. 9 and 10 demonstrate the velocity as well as temperature fields for the increment ($0.05 \leqslant (\gamma = \gamma_A) \geqslant 0.35$) of dimensionless fourth-grade fluid parameters (γ and γ_A). Velocity profiles decrease, and temperature profiles develop for the increment in fourth-grade fluid parameter (γ and γ_A). Variations of concentric fields are exhibited for different values of K_r with considering the order p = 4.

Due to the rise in a destructive chemical reaction (K_r) parameter from $0.50 \leqslant Kr \geqslant 10.0$, the concentration fields get decrease (Fig. 11). Physically, a destructive chemical reaction occurs with more disturbances which develops the molecular motion and upsurges the heat transport phenomena, as a result the concentric profiles diminish. Fig. 12 is plotted to visualise the impression of Prandtl number (P_r) on θ. The parameter (P_r) is the proportion of kinematic viscosity and thermal diffusivity which changes physically with temperature. For instance, water P_r = 7.0 (At 20 °C) and Ammonia gases P_r = 1.38 decline more rapidly than air P_r = 0.71. However, $P_r \ll 1$ and $P_r \gg 1$ depict the domination of thermal and momentum diffusivity respectively. Prandtl number is used roughly to determine whether heat transport occurs with either conduction or convection process. Since, Prandtl number is inversely proportional to thermal diffusivity so that increasing P_r led the temperature profiles to decrease.

Thermal radiation is known as electromagnetic radiation or the conversion of thermal energy, which generates the thermal motion

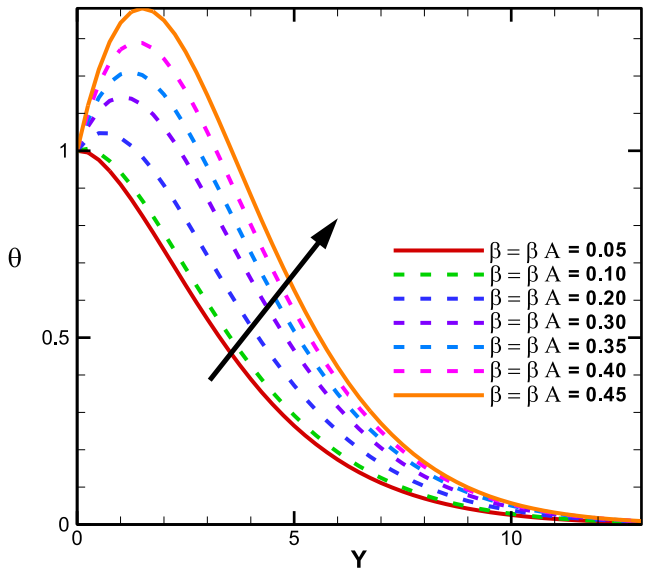

Fig. 8. Dominance of β and β_A on θ.

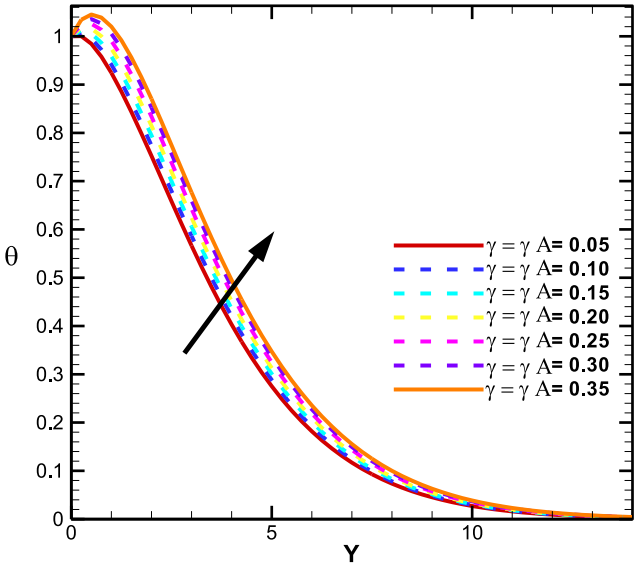

Fig. 10. Dominance of γ and γ_A on θ.

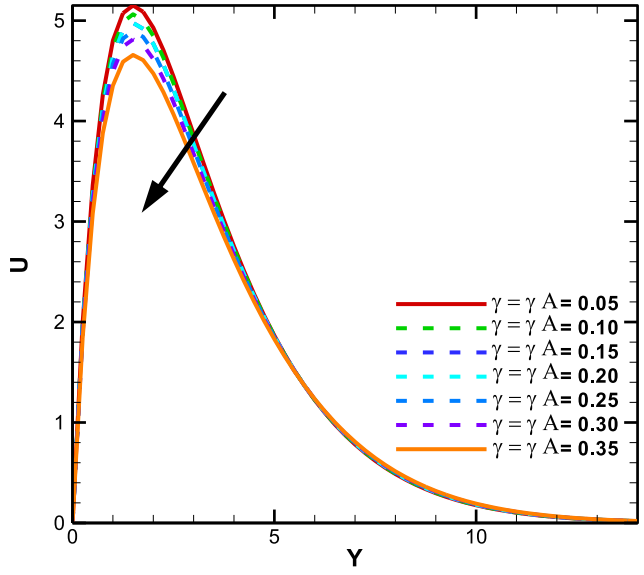

Fig. 9. Dominance of γ and γ_A on U.

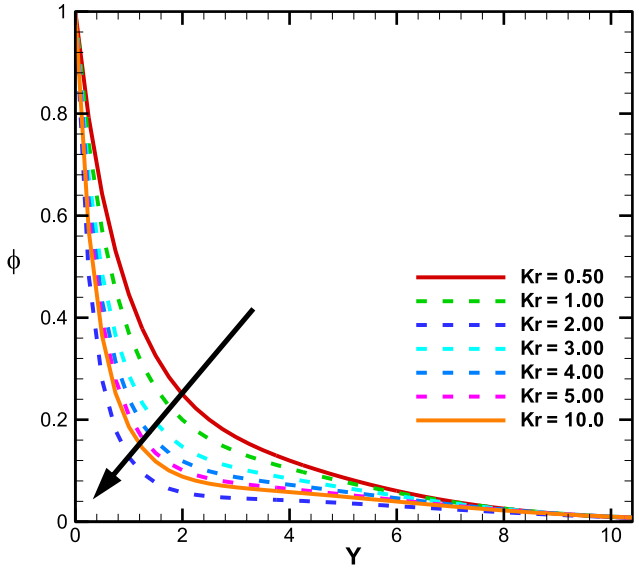

Fig. 11. Dominance of K_r on φ.

of particles in matter. Thermal radiation (electromagnetic radiation) could be attributed due to thermal excitation. The temperature could be affected in the presence of thermal radiation at moderate temperatures which are significant. Thermal radiation for a medium which contains it inevitably has pressure and density gradients, and the treatment requires the use of hydrodynamics. Fig. 13 display the variations of Nusselt number profiles for different data of thermal radiation (R) parameter. It is seen that, with the increase ($0.05 \leqslant R \geqslant 0.70$) of R, the Nusselt number profiles are also increasing. Because for larger values of R the mean absorption coefficient get declines and accelerates the divergence of heat flux. Here, the curve to curve fluctuations are 20.64%, 13.92%, 10.35%, 8.57%, 7.28% and 6.28% when the value of R are changes from 0.05 to 0.70 with the following data 1.1993, 1.21994, 1.24082, 1.25117, 1.25974, 1.26702 and 1.27330 respectively. Fig. 14 represents the Sherwood number profiles for the increment of Schmidt number. For the data of $S_c = (2.0–6.0)$, S_h profiles increase but decrease for $S_c = 8.0$ and again increase for the values of Sc ($8.0 \leqslant Sc \geqslant 14.0$). Physically, Schmidt number helps to develop the fluid concentration as well as the concentration buoyancy force. Furthermore, streamlines and isotherms profiles can be used to improve the visualisation of fluid fields. Here, the line view is presented to explain the influence of thermal radiation on streamlines and isotherms. In Figs. 15 and 16 represent the thermal and velocity boundary layer from 0 to $+X$ the region for X-axis through the vertical plate. It can be seen that thermal and momentum boundary layers increase within the flow region for strong thermal radiation (R) with $\tau = 0$ to 30 non-dimensional time steps.

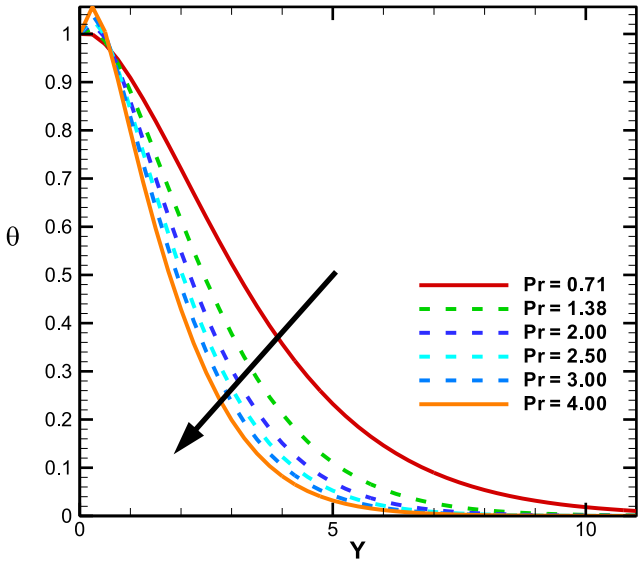

Fig. 12. Dominance of P_r on θ.

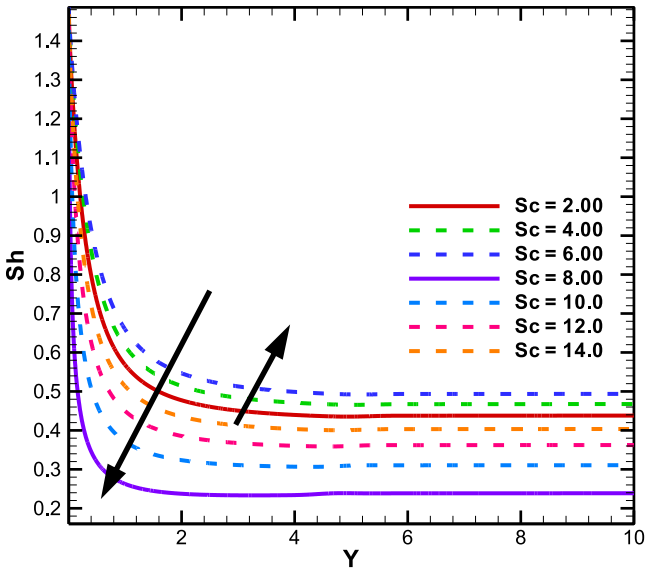

Fig. 14. Dominance of S_c on S_h.

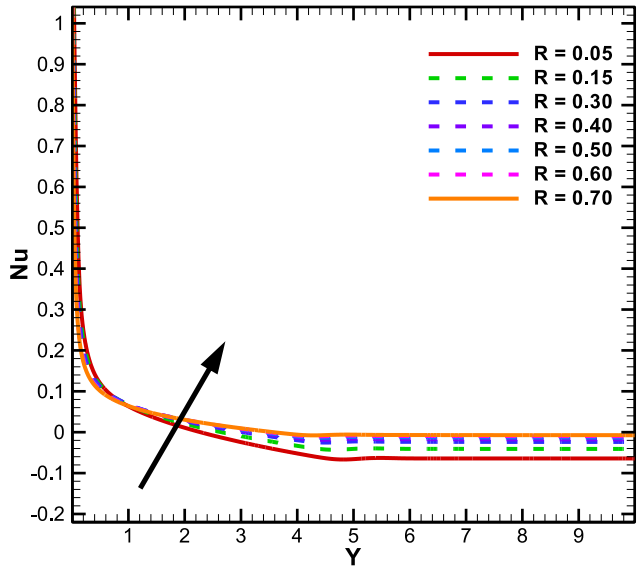

Fig. 13. Dominance of R on N_u.

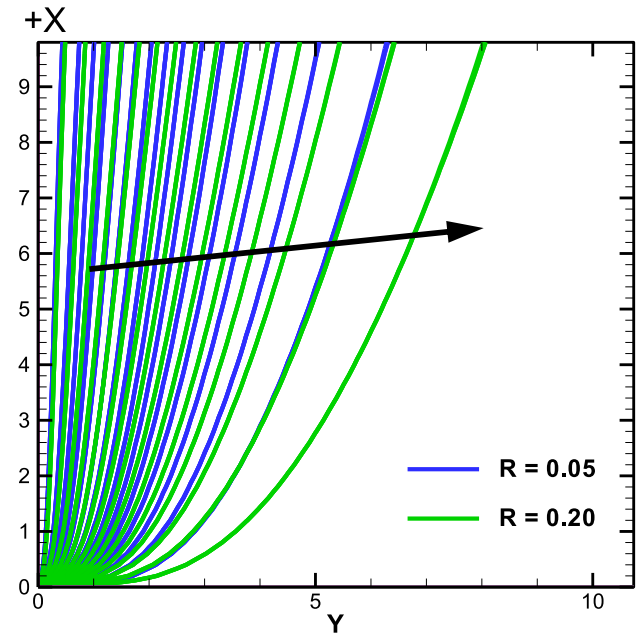

Fig. 15. Isotherms for different data of R with $\tau = 10$ to 30 time steps.

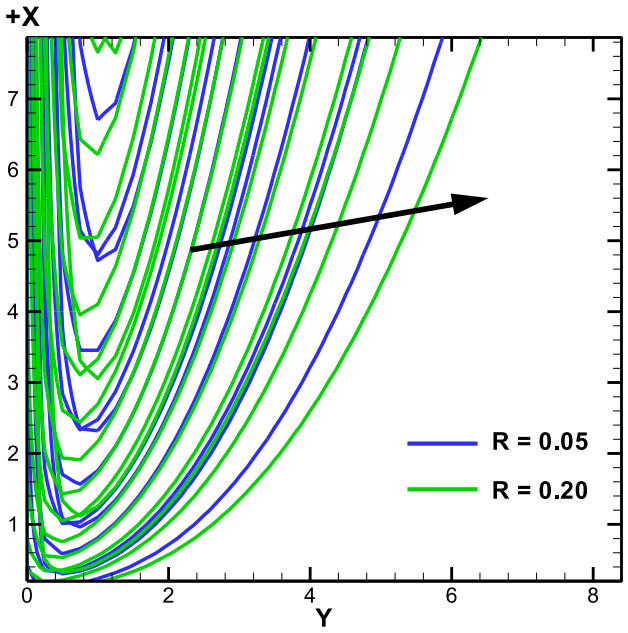

Fig. 16. Streamlines for different data of R with $\tau = 10$ to 30 time steps.

6. Conclusions

The numerical solution for fourth-grade fluid towards an infinite vertical porous plate with chemical reaction, thermal radiation, heat source, uniform suction, MHD, streamlines and isotherm lines representation has been analysed. The key findings are given below:

- Velocity and skin friction fields decline due to the increment in magnetic parameter.
- Velocity profiles decrease, and temperature fields go up when dimensionless second, third and fourth-grade parameters get to raise.
- For upsurging data of destructive chemical reaction concentric fields diminish.
- Increasing Prandtl numbers tend to diminish the temperature profiles.
- Nusselt number distribution rises due to the enhancement in thermal radiation.
- Strong values of Schmidt number increase the boundary layers in Sherwood number fields.
- Higher values of thermal radiation expand the thickness of thermal and momentum boundary layers in streamline and isothermal lines.

References

Arifuzzaman, S.M., Biswas, P., Mehedi, M.F.U., Ahmmed, S.F., Khan, M.S., 2018a. Analysis of unsteady boundary layer viscoelastic nanofluid flow through a vertical porous plate with thermal radiation and periodic magnetic field. J. Nanofluids 7, 1122–1129.

Arifuzzaman, S.M., Khan, M.S., Hossain, K.E., Islam, M.S., Akter, S., Roy, R., 2017a. Chemically reactive viscoelastic fluid flow in presence of nano particle through porous stretching sheet. Front. Heat Mass Transf. 9, 1–14.

Arifuzzaman, S.M., Khan, M.S., Islam, M.S., Islam, M.M., Rana, B.M.J., Biswas, P., Ahmmed, S.F., 2017b. MHD Maxwell fluid flow in presence of nano-particle through a vertical porous–plate with heat-generation, radiation absorption and chemical reaction. Front. Heat Mass Transf. 9, 1–14.

Arifuzzaman, S.M., Khan, M.S., Mehedi, M.F.U., Rana, B.M.J., Ahmmed, S.F., 2018b. Chemically reactive and naturally convective high speed MHD fluid flow through an oscillatory vertical porous plate with heat and radiation absorption effect. Eng. Sci. Technol. Int. J. 21, 215–228.

Arifuzzaman, S.M., Rana, B.M.J., Ahmed, R., Ahmmed, S.F., 2017c. Cross diffusion and MHD effects on a high order chemically reactive micropolar fluid of naturally convective heat and mass transfer past through an infinite vertical porous medium with a constant heat sink. AIP Conf. Proc. 1851, 020006.

Asghar, S., Hanif, K., Hayat, T., Khalique, C.M., 2007. MHD non-Newtonian flow due to non-coaxial rotations of an accelerated disk and a fluid at infinity. Commun. Nonlinear Sci. Numer. Simul. 12, 465–485.

Aziz, T., Mahomed, F.M., 2013. Reductions and solutions for the unsteady flow of a fourth grade fluid on a porous plate. Appl. Math. Comput. 219, 9187–9195.

Bhatti, M.M., Rashidi, M.M., 2016. Effects of thermo-diffusion and thermal radiation on Williamson nanofluid over a porous shrinking/stretching sheet. J. Mol. Liq. 221, 567–573.

Bhatti, M.M., Zeeshan, A., Ellahi, R., Shit, G.C., 2018. Mathematical modeling of heat and mass transfer effects on MHD peristaltic propulsion of two-phase flow through a Darcy-Brinkman-Forchheimer porous medium. Adv. Powder Technol. 29, 1189–1197.

Biswas, P., Arifuzzaman, S.M., Karim, I., Khan, M.S., 2017. Impacts of magnetic field and radiation absorption on mixed convective jeffrey nano fluid flow over a vertical stretching sheet with stability and convergence analysis. J. Nanofluids 6, 1082–1095.

Biswas, P., Arifuzzaman, S.M., Khan, M.S., 2018. Effects of periodic magnetic field on 2D transient optically dense gray nanofluid over a vertical plate: a computational EFDM study with SCA. J. Nanofluids 7, 1–10.

Coleman, B.D., Noll, W., 1960. An approximation theorem for functionals with applications in continuum mechanics. Arch. Ration. Mech. Anal. 6, 355–370.

Eldabe, N.T., Elogail, M.A., Elshaboury, S.M., Hasa, A.A., 2016. Hall effects on the peristaltic transport of Williamson fluid through a porous medium with heat and mass transfer. Appl. Math. Model. 40, 315–328.

Eldahab, E.M., Salem, A.M., 2005. MHD free-convection flow of a non-Newtonian power-law fluid at a stretching surface with a uniform free-stream. Appl. Math. Comput. 169, 806–818.

Ellahi, R., Alamri, S.Z., Basit, A., Majeed, A., 2018a. Effects of MHD and slip on heat transfer boundary layer flow over a moving plate based on specific entropy generation. J. Taibah Univ. Sci. 12, 476–482.

Ellahi, R., Zeeshan, A., Shehzad, N., Alamri, S.Z., 2018b. Structural impact of kerosene-Al_2O_3 nanoliquid on MHD Poiseuille flow with variable thermal conductivity: application of cooling process. J. Mol. Liq. 264, 607–615.

Ezzat, M.A., 2010. Thermoelectric MHD non-Newtonian fluid with fractional derivative heat transfer. Physica B Condens. Matter. 405, 4188–4194.

Fetecau, C., Ellahi, R., Khan, M., Shah, N.A., 2018. Combined porous and magnetic effects on some fundamental motions of Newtonian fluids over an infinite plate. J. Porous Media 21, 589–605.

Gul, T., Ghani, F., Islam, S., Shah, R.A., Khan, I., Nasir, S., Sharidan, S., 2016. Unsteady thin film flow of a fourth grade fluid over a vertical moving and oscillating belt. Propul. Power Res. 5, 223–235.

Hassan, M., Faisal, A., Bhatti, M.M., 2018a. Interaction of aluminum oxide nanoparticles with flow of polyvinyl alcohol solutions base nanofluids over a wedge. Appl. Nanoscience 8, 53–60.

Hassan, M., Marin, M., Alsharif, A., Ellahi, R., 2018b. Convective heat transfer flow of nanofluid in a porous medium over wavy surface. Phys. Lett. A.

Hassan, M., Zeeshan, A., Majeed, A., Ellahi, R., 2017. Particle shape effects on ferrofuids flow and heat transfer under influence of low oscillating magnetic field. J. Magn. Magn. Mater. 443, 36–44.

Hayat, T., Naz, R., Abbasbandy, S., 2011. On flow of a fourth-grade fluid with heat transfer. Int. J. Numer. Meth. Fluids 67, 2043–2053.

Hayat, T., Wang, Y., Hutter, K., 2002. Flow of a fourth grade fluid. Math. Models Methods Appl. Sci. 12, 797–811.

Hussain, F., Ellahi, R., Zeeshan, A., 2018. Mathematical models of electro-magnetohydrodynamic multiphase flows synthesis with nano-sized hafnium particles. Appl. Sci. 8, 3–18.

Khan, A.A., Masood, F., Ellahi, R., Bhatti, M.M., 2018. Mass transport on chemicalized fourth-grade fluid propagating peristaltically through a curved channel with magnetic effects. J. Mol. Liq. 258, 186–195.

Khan, M.S., Karim, I., Ali, L.E., Islam, A., 2012a. Unsteady MHD free convection boundary-layer flow of a nanofluid along a stretching sheet with thermal radiation and viscous dissipation effects. Int. Nano Lett. 2, 24.

Khan, M.S., Karim, I., Biswas, M.H.A., 2012b. Non-Newtonian MHD mixed convective power-law fluid flow over a vertical stretching sheet with thermal radiation, heat generation and chemical reaction effects. Acad. Res. Int. 3, 80–92.

Khan, M.S., Rahman, M.M., Arifuzzaman, S.M., Biswas, P., Karim, I., 2017. Williamson fluid flow behaviour of MHD convective-radiative Cattaneo-Christov heat flux type over a linearly stretched-surface with heat generation and thermal-diffusion. Front. Heat Mass Transf. 9, 1–11.

Li, J., Liu, L., Zheng, L., Bin-Mohsin, B., 2016. Unsteady MHD flow and radiation heat transfer of nanofluid in a finite thin film with heat generation and thermophoresis. J. Taiwan Inst. Chem. Eng. 67, 226–234.

Majeed, A., Zeeshan, A., Alamri, S.Z., Ellahi, R., 2018. Heat transfer analysis in ferromagnetic viscoelastic fluid flow over a stretching sheet with suction. Neural Comput. Appl. 30, 1947–1955.

Mishra, S., Pattnaik, P., Bhatti, M., Abbas, T., 2017. Analysis of heat and mass transfer with MHD and chemical reaction effects on viscoelastic fluid over a stretching sheet. Indian J. Phys. 91, 1219–1227.

Reza-E-Rabbi, S., Arifuzzaman, S.M., Sarkar, T., Khan, M.S., Ahmmed, S.F., 2018. Explicit finite difference analysis of an unsteady MHD flow of a chemically reacting Casson fluid past a stretching sheet with Brownian motion and thermophoresis effects. J. King Saud University-Sci. in press.

Sahoo, B., Poncet, S., 2013. Blasius flow and heat transfer of fourth-grade fluid with slip. Appl. Math. Mech. 34, 1465–1480.
Shahid, A., Bhatti, M., Bég, O.A., Kadir, A., 2017. Numerical study of radiative Maxwell viscoelastic magnetized flow from a stretching permeable sheet with the Cattaneo-Christov heat flux model. Neural Comput. Appl., 1–12
Shahid, A., Zhou, Z., Hassan, M., Bhatti, M.M., 2018. Computational study of magnetized blood flow in the presence of Gyrotactic microorganisms propelled through a permeable capillary in a stretching motion. Int. J. Multiscale Comput. Eng. 16, 303–320.
Shehzad, N., Zeeshan, A., Ellahi, R., 2018. Electroosmotic flow of MHD power law Al_2O_3-PVC nanouid in a horizontal channel: couette-poiseuille flow model. Commun. Theor. Phys. 69, 655–666.
Srinivasa, A.H., Eswara, A.T., 2016. Effect of internal heat generation or absorption on MHD free convection from an isothermal truncated cone. Alexandria Eng. J. 55, 1367–1373.
Umamaheswar, M., Raju, M.C., Varma, S.V.K., Gireeshkumar, J., 2016. Numerical investigation of MHD free convection flow of a non-Newtonian fluid past an impulsively started vertical plate in the presence of thermal diffusion and radiation absorption. Alexandria Eng. J. 55, 2005–2014.
Wang, Y., Wu, W., 2007. Unsteady flow of a fourth grade fluid due to an oscillation plate. Int. J. Non Linear Mech. 42, 432–441.
Zeeshan, A., Ijaz, N., Abbas, T., Ellahi, R., 2018. The sustainable characteristic of bio-bi-phase flow of peristaltic transport of MHD Jeffrey fluid in the human body. Sustainability 10, 1–17.